REPORT DOCUMENTATION PAGE

Public Reporting burden for this collection of information is estimated to average 1 hour per response, including the time for reviewing instructions, searching existing data sources, gathering and maintaining the data needed, and completing and reviewing the collection of information. Send comment regarding this burden estimates or any other aspect of this collection of information, including suggestions for reducing this burden, to Washington Headquarters Services, Directorate for information Operations and Reports, 1215 Jefferson Davis Highway, Suite 1204, Arlington, VA 22202-4302, and to the Office of Management and Budget, Paperwork Reduction Project (0704-0188,) Washington, DC 20503.

1. AGENCY USE ONLY (Leave Blank)	2. REPORT DATE November 15, 2003	3. REPORT TYPE AND DATES COVERED Final Report, Jan 1, 1993 to Aug 15, 2003

4. TITLE AND SUBTITLE
Failure Prediction of Underwater Structures – Subdomain Decomposition and Meshfree Methods

5. FUNDING NUMBERS
N00014-93-1-0292

6. AUTHOR(S)
Ted Belytschko

7. PERFORMING ORGANIZATION NAME(S) AND ADDRESS(ES)
Northwestern University, Department of Mechanical Engineering, 2145 Sheridan Road, Illinois, 60208-3111

8. PERFORMING ORGANIZATION REPORT NUMBER 0650-350-N484

9. SPONSORING / MONITORING AGENCY NAME(S) AND ADDRESS(ES)
Office of Naval Research
800 N Quincy St
Arlington, VA 22217-5600

10. SPONSORING / MONITORING AGENCY REPORT NUMBER

11. SUPPLEMENTARY NOTES
The views, opinions and/or findings contained in this report are those of the author(s) and should not be construed as an official Department of the Navy position, policy or decision, unless so designated by other documentation.

12 a. DISTRIBUTION / AVAILABILITY STATEMENT
Approved for public release; distribution unlimited.

12 b. DISTRIBUTION CODE

13. ABSTRACT (Maximum 200 words)

Meshfree methods for fracture have been extended by considering more general classes of basis functions. These methods do not require any elements, and boundaries and interfaces, such as cracks, are easy to propagate in the model since it does not involve remeshing. The versatility of these methods has been enhanced by developing new vector level set methods. The method has been applied to a variety of crack growth problems in two dimensions including problems involving welds and fillets. Comparisons with experiments show excellent agreement. Domain decomposition methods, whereby a fine scale model can be linked with a coarse scale model were developed. These methods are useful when a part of a ship where severe damage is expected must be modeled by a refined mesh for accuracy and linked to a coarser mesh of the remainder of the ship.

14. SUBJECT TERMS
meshless methods, finitie element methods, crack growth

15. NUMBER OF PAGES
5 pages

16. PRICE CODE

17. SECURITY CLASSIFICATION OR REPORT UNCLASSIFIED	18. SECURITY CLASSIFICATION ON THIS PAGE UNCLASSIFIED	19. SECURITY CLASSIFICATION OF ABSTRACT UNCLASSIFIED	20. LIMITATION OF ABSTRACT UL

NSN 7540-01-280-5500

Standard Form 298 (Rev.2-89)
Prescribed by ANSI Std. 239-18
298-102

20031217 208

<div style="border: 1px solid black;">

REPORT DOCUMENTATION PAGE (SF298)
(Continuation Sheet)

</div>

Final Report on

Failure Prediction of Underwater Structures – Subdomain Decomposition and Meshfree Methods

By

Ted Belytschko
Northwestern University
Department of Mechanical Engineering
2145 Sheridan Road
Evanston, IL 60208-3111
Phone: 847.491.4029
Fax: 847.491.3915
Email: tedbelytschko@northwestern.edu

Jan 1, 1993 to Aug 15, 2003

Failure Prediction of Underwater Structures – Subdomain Decomposition and Meshfree Methods

Preface

This award supported research of Failure Prediction of Underwater Structures – Subdomain Decomposition and Meshfree Methods. Professor Ted Belytschko directed this research. The following individuals were supported by this research: T. Black, Nicolas Moes, S. Usui, Jack Chessa, Hongwu Wang, Furio Stazi, Elisa Budyn, and Jingxiao Xu.

The following papers were published to report the results of this research under the support of this grant:

T. Belytschko, K. Mish, "Computability in non-linear solid mechanics," International Journal for Numerical Methods in Engineering, 52:3-21 (2001)

T Belytschko, S Xiao, "Stability Analysis of Particle Methods with Corrected Derivatives," Computers & Mathematics with Applications, 43: 329-350 (2002)

S Li, WK Liu, AJ Rosakis, T Belytschko, W Hao, "Mesh-free Galerkin simulations of dynamic shear band propagation and failure mode transition," International Journal of Solids and Structures, 39: 1213-1240 (2002)

S. Li, D. Qian, W.K. Liu, T. Belytschko, "A meshfree contact-detection algorithm," Computer Methods in Applied Mechanics and Engineering, 190: 3271-3292 (2001)

J.T. Oden, T. Belytschko, I. Babuska, T.J.R. Hughes, "Research directions in computational mechanics," Computer Methods in Applied Mechanics and Engineering, 192: 913-922 (2003)

G Ventura, JX Xu, T Belytschko, "A vector level set method and new discontinuity approximations for crack growth by EFG," International Journal for Numerical Methods in Engineering, 54 (6): 923-944 (2002)

MASTER COPY: PLEASE KEEP THIS "MEMORANDUM OF TRANSMITTAL" BLANK FOR REPRODUCTION PURPOSES. WHEN REPORTS ARE GENERATED UNDER THE ONR SPONSORSHIP, FORWARD A COMPLETED COPY OF THIS FORM WITH EACH REPORT SHIPMENT TO THE ONR. THIS WILL ASSURE PROPER IDENTIFICATION. <u>NOT TO BE USED FOR</u> <u>INTERIM PROGRESS REPORTS</u>; SEE PAGE 2 FOR INTERIM PROGRESS REPORT INSTRUCTIONS.

<u>MEMORANDUM OF TRANSMITTAL</u>

Office of Naval Research
536 S. Clark Street, Room 208
Chicago, IL 60605-1588

☐ Reprint (Orig + 2 copies)   ☐ Technical Report (Orig + 2 copies)

☐ Manuscript (1 copy)   xx☐ Final Progress Report (Orig + 2 copies)

                                    ☐ Related Materials, Abstracts, Theses (1 copy)

CONTRACT/GRANT NUMBER: Contract No. 0650-350-N484

REPORT TITLE: Failure Prediction of Underwater Structures – Subdomain Decomposition and Meshfree Methods

is forwarded for your information.

SUBMITTED FOR PUBLICATION TO (applicable only if report is manuscript):

Failure Prediction of Underwater Structures- Subdomain Decomposition and Meshfree Methods

By Ted Belytschko

Introduction:

Meshfree methods for fracture have been extended by considering more general classes of basis functions. These methods do not require any elements, and boundaries and interfaces, such as cracks, are easy to propagate in the model since it does not involve remeshing. The versatility of these methods has been enhanced by developing new vector level set methods. In these methods, the crack is represented entirely by vector functions at the nodes of the meshless model. Therefore, there is no need for alternative representations of the crack as it evolves. This extra data is only needed at nodes in a subdomain around the crack. The method has been applied to a variety of crack growth problems in two dimensions including problems involving welds and fillets. Comparisons with experiments show excellent agreement. Extensions of the method to three dimensions are now under development. Further studies have been made of the stability of particle forms of meshless methods. It has been shown that in two dimensions the widely used Eulerian kernels distort the onset of material instability and often manifest instabilities that look like material instabilities. It has also been shown that Lagrangian kernels that were proposed earlier in this grant do not distort the onset of material instabilities.

Domain decomposition methods, whereby a fine scale model can be linked with a coarse scale model, are being developed. These methods are useful when a part of a ship where severe damage is expected must be modeled by a refined mesh for accuracy and linked to a coarser mesh of the remainder of the ship. The method that has been developed is based on an overlapping domain decomposition method. Part of the fine scale subdomain overlaps the coarse scale subdomain. In each time step, the fine scale solution is projected on the coarse scale solution so that spurious reflections on the interface are prevented. Methods have also been developed in which a smaller time step can be used in the fine scale subdomain. The method has been studied in model one and two-dimensional problems. Results show that spurious reflections are almost totally eliminated.

1. Stability of Meshless Methods based on Lagrangian and Eulerian kernels

A major difficult of meshless methods such as SPH and EFG has been the appearance of a so-called tensile instability. We have shown that the tensile instability is even more pervasive than it appears at first, for it drastically changes the stable material domain. Therefore, the prediction of cracks or shear bands by a meshless method with a distorted material stability domain can lead to highly erroneous results. In the following we show the analysis which has led us to that conclusion. We also propose a remedy, the use of Lagrangian kernels.

An isotropic hyperelastic material model is used the study the domain of material stability. Its potential is given by

$$\psi = \frac{1}{2}c_1I_1 + \frac{1}{2}c_2I_2 - \left[\frac{3}{2}c_1I_3^{\frac{1}{3}} + \frac{3}{2}c_2I_3^{\frac{2}{3}} - \frac{\lambda}{4}(\ln I_3)^2\right] \tag{1.1}$$

where c_1 and c_2 are constants. I_1, I_2 and I_3 are the principal invariants of the right Cauchy-Green deformation tensor $\mathbf{C}$.

Based on a linearized stability analysis the material instability in the continuum is given. Fig. 1.1 shows the stable domain of continuum. We call the stable domain as calculated for the partial differential equation the "exact" stable domain, even though it is obtained numerically.
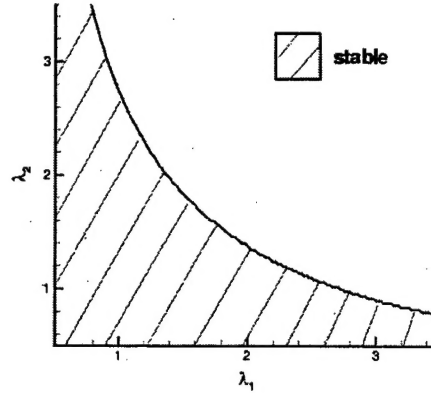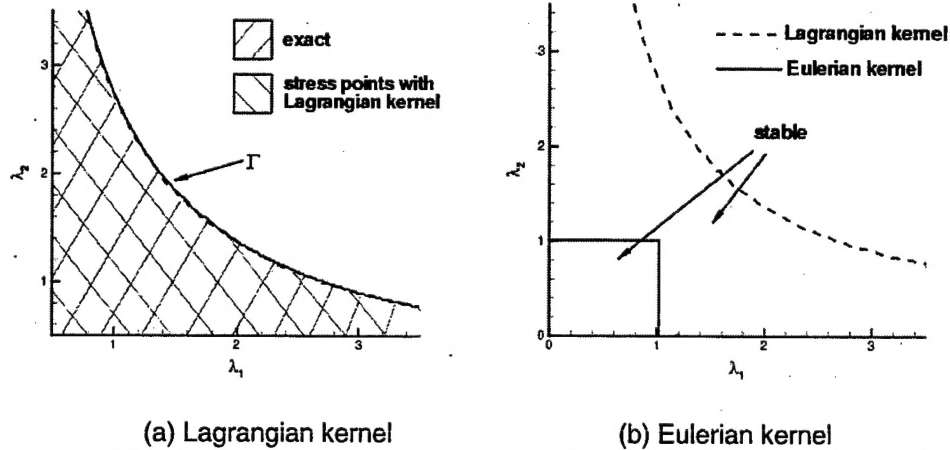

Fig. 1.1 : The stable domain of continuum

(a) Lagrangian kernel   (b) Eulerian kernel

Fig. 1.2 : Stable domain of particle methods with stress point integration

We studied the material instability for particle methods with either Lagrangian kernel or Eulerian kernel. Fig. 1.2(a) shows that Lagrangian kernel can exactly reproduce the material instability. When Eulerian kernel is used, the material instability is distorted severely as shown in Fig. 1.2(b).

As a compressible, homogeneous and isotropic, elastic material proposed by Blatz and Ko, Blatz-Ko material has the following potential function

$$W(I_1, I_2, I_3) = \frac{\mu}{2}\left(I_2 J^{-2} + 2J - 5\right) \tag{1.2}$$

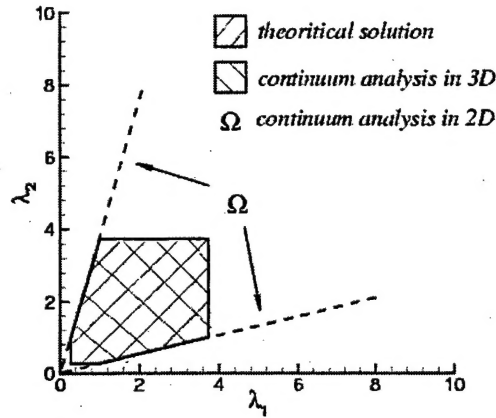where $J = \sqrt{I_3}$ and μ is a constant.

Fig. 1.3: Stable domain from theoretical solution compared with the solution from PDE
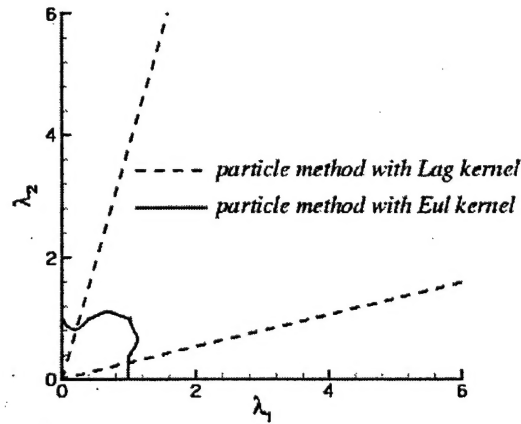

Fig. 1.4: Stable domain calculated from particle methods

Knowles and Sternberg gave the stable criteria for Blatz-Ko material by an analysis of the associated issue of ellipticity. The stable domain is a hexagon which is shown in Fig. 1.4. The linearized stability analysis is used as before in continuum and particle methods to study the stable domain, compared to the theoretical solution. When we use the two-dimensional stability analysis for the continuum, the stable domain is located between the two rays from the original point as shown in Fig. 1.4. It is identical to the stable domain in Fig. 1.4, which is calculated from the particle methods with Lagrangian kernel. Fig. 1.4 also shows that the stable domain is extremely distorted when calculated from the particle methods with Eulerian kernel.

2. Effect of Cohesive Laws on Crack

In order to study cohesive cracks, we have developed a new enrichment techniques by which curved cohesive cracks can be treated with higher order enrichments. The crack tip can be located anywhere within an element. The technique is based on Chen's (2003) development for constant strain triangles and extended to quadratic elements. An essential feature in applying the method to the static cohesive crack model is that the crack opening should be quadratic in the vicinity of the crack tip.

Moes and Belytschko (2002) implemented the XFEM scheme for cohesive cracks in linear triangular elements. In their work, a linear element is enriched by the step function if it is completely cut by a crack, and by the branch function if the crack tip is located inside the element.

3

In the enrichment developed here, an element containing a crack tip is enriched by the step function whose gradient is normal to the crack and a polynomial along the crack. We consider polynomials of first and second order but the method is applicable to any order. The contribution of the paper lies in that the branch function used in previous XFEM (Moes and Belytschko 2002) formulations for cracks is dropped, so that the partition of unity holds in the entire enriched subdomain. It is shown that this yields good stress results near the crack tip for cohesive crack models. Both a first order scheme and a second order scheme are developed by this procedure. The scheme can be applied to various nonlinear softening laws.

Branch functions, typically, $r^m \sin(\vartheta/2)$ where $m = 0.5, 2.0$, etc., have been used for the enrichment of the tip element (Belytschko and Black 1999; Moes and Belytschko 2002; Stazi et al. 2003). For a discussion of the branch function, see Belytschko et al. (2001). When branch functions are used in conjunction with step functions, as in Moes et al. (1999), the partition of unity property does not hold in the elements surrounding the tip element. The enrichment of those elements is a local partition of unity and it must be blended to the rest of the domain for optimal performance because the branch function does not vanish at the edges of the tip element. Note that the branch function is not a piecewise constant function like the sign function. For a discussion of local partitions of unity and blending, see Chessa et al. (2003).

In order to avoid the difficulties associated with the branch functions in the tip element, a new enrichment has been developed. This procedure is similar to that given by Chen (2003) but it is generalized to quadratic elements in this work. It can be applied to elements of any order without difficulty.
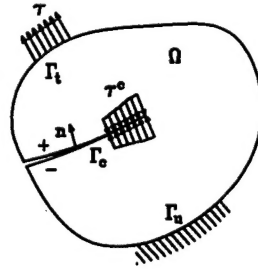

Fig. 2.1: A two dimensional domain containing a cohesive crack inside the domain.

Consider a crack Γ_c in a two dimensional body Ω with boundary Γ as shown in Fig. 2.2. We denote by x the spatial coordinates. The crack is described implicitly by the level set function $\phi(x) = 0$ and its two end points x_I, $I = 1,2$. Depending on the cohesive law, a traction τ_c is applied across the crack surface near the tip.

The displacement field u of the body can be additively decomposed into a continuous part u_{cont} and a discontinuous part u_{disc}: $u(x) = u_{cont}(x) + u_{disc}(x)$. The discontinuous part of the displacement field is approximated by standard shape functions $N_I(x)$, so

$$u_{cont}(x) = \sum_{I \in N_{tot}} N_I(x) u_I \tag{2.1}$$

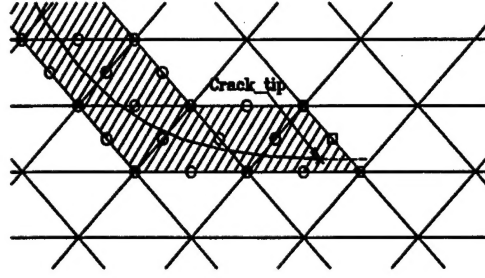where N_{tot} is the total set of nodes and u_I are nodal displacements.

Fig. 2.2: The enriched domain Ω_{enr} (shaded area) and the enriched nodes N_{enr} (circles), where a virtual (dashed) line segment is added to calculate the signed distance function in the tip element; at square nodes, the enrichment parameters $a_I = 0$

If we consider a triangulation on the body Ω as shown in Fig. 2.2, then the discontinuous part of the displacement field can be limited to the elements that contain the crack. We call this subdomain Ω_{enr}.

Let N_{enr} be the set of nodes of the elements cut by the crack Γ_c. The discontinuous part of the displacement field can then be written as (Belytschko and Black 1999).

$$u_{disc}(x) = \sum_{I \in N_{enr}} N_I(x) \Psi_I(x) a_I \qquad (2.2)$$

where $\Psi_I(x) = sign(\phi(x)) - sign(\phi_I)$ and a_I are enrichment parameters.
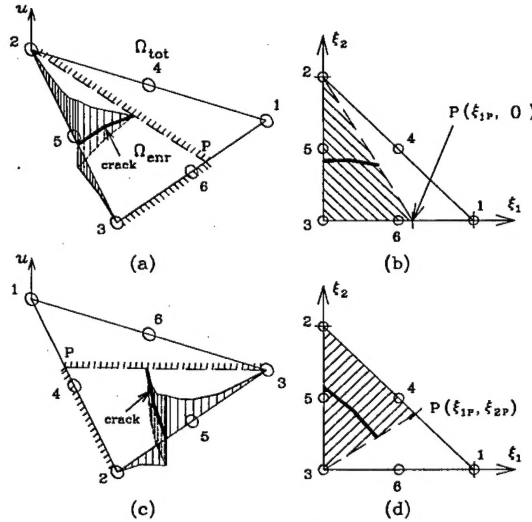

Fig. 2.3: Enrichment displacement field u_{disc} in a 6-node quadratic tip element for two crack directions and the corresponding parent domains; the shaded areas represent the enriched region Ω_{enr}.

The enrichment developed for a 3-node element by Chen (2003) is generalized to a 6-node element (Fig. 3) as follows. We consider an element where the crack passes through side 24. Let the direction of the crack be such that it intersects side 13. Other relationships between the element and the crack can be obtained by permuting the node numbers. We wish to construct an enrichment that vanishes on the two edges 12 and 13 (which is necessary for compatibility), and is continuous across edge 23 with the field in the adjacent element. To meet these conditions, only nodes 3, 5, 6 are enriched and the discontinuous displacement field in the tip element is

5

$$u_{disc} = N_3(\xi^*)\Psi_3(\xi^*)a_3 + N_5(\xi^*)\Psi_5(\xi^*)a_5 + N_6(\xi^*)\Psi_6(\xi^*)a_6 \tag{2.3}$$

where ξ^* are the parent coordinates of the shaded region 23P in Fig. 3b, i.e. the element generated by side 23, side 3 P and P2, where P is the intersection point of the line joining node 2 to the crack tip and side 32. The shaded parent area coordinates are related by $\xi_3^* = 1 - \xi_1^* - \xi_2^*$ and

$\Psi_3(\xi^*) = sign(\phi(\xi^*)) - sign(\phi_3)$. The relation between ξ^* and ξ is given by

$$\xi_1^* = \frac{\xi_1}{\xi_{1P}} \quad \text{and} \quad \xi_2^* = \xi_2 \tag{2.4}$$

where ξ_{1P} is the area coordinate of point P.

When the direction of the crack intersects side 31 (Fig. 3c,d), then the discontinuous part of the displacement field is

$$u_{disc} = N_2(\xi^*)\Psi_2(\xi^*)a_2 + N_4(\xi^*)\Psi_4(\xi^*)a_4 + N_5(\xi^*)\Psi_5(\xi^*)a_5 \tag{2.5}$$

where

$$\xi_1^* = \xi_1 - \frac{\xi_{1P}}{\xi_{2P}}\xi_2 \quad \text{and} \quad \xi_2^* = \frac{\xi_2}{\xi_{2P}} \tag{2.6}$$

Based on the preceding, we can simply write the discontinuous displacement of a quadratic tip element as

$$u_{disc} = \sum_{I \in N_{enr,tip}} N_I(\xi^*)\Psi_I(\xi)a_I \tag{2.7}$$

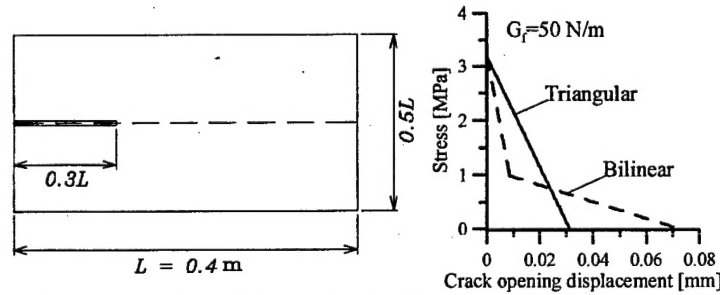with $a_I = 0$ at three of the nodes as shown in Fig. 2.3.

Fig. 2.4: A double cantilever-beam (DCB) with 30% notch and linear and bilinear softening laws.

In order to study the new XFEM scheme, we solved the double-cantilever-beam (DCB) problem shown in Fig. 2.4; a linear softening law is used. Young's modulus is 36.5 GPa and Poisson's ratio is 0.18. The results obtained by the new XFEM scheme are compared to those obtained by the static condensation method (e.g. Zi and Bazant 2003) which has extensively been used to analyze the fracture properties of many experimental tests when the direction of crack propagation is known. The static condensation method is also known as the pseudo boundary integral (PBI) method.

The weak form and the discretized equation of equilibrium are similar to Moes and Belytschko's (2002), so it is omitted here. But, the condition that the stress at the crack tip should be equal to the tensile strength is used instead of the zero stress intensity factor for its simplicity. The equilibrium condition and the stress condition are solved simultaneously by the Newton-Raphson method.
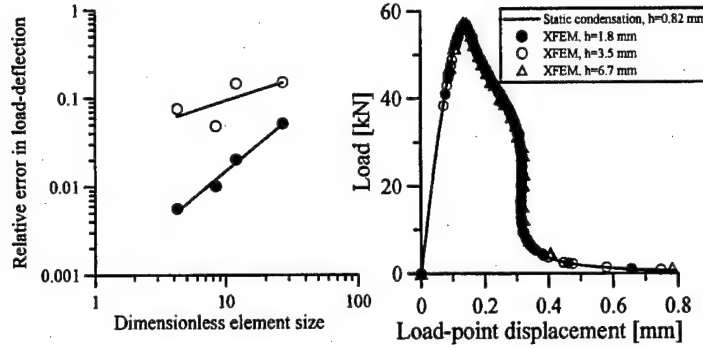
Fig. 2.5: Relative errors in load-deflection histories obtained by the extended finite element methods with linear elements (empty circles) and quadratic elements (solid circles).

The convergence rates for the linear and quadratic elements for various mesh refinements are shown in Fig. 2.5 (left). The convergence rate of the second order method, 2.23, is much better than the first order method, 0.48, respectively.

The load-deflection histories for the quadratic elements with the stress condition are plotted and compared to the result by the static condensation method in Fig. 2.5 (right). The load deflection histories are calculated for three different mesh refinements and, for all cases, agree well with the reference.
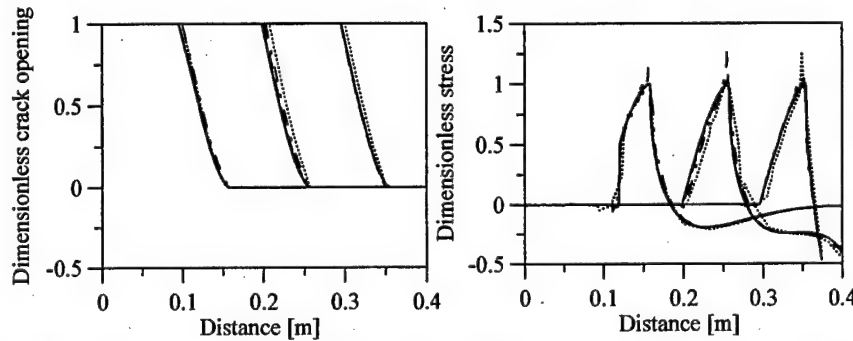

Fig. 2.6: Comparison of dimensionless crack opening and stresses σ_y by the XFEM method (dashed line: h=2 mm, dash-dot line: h=5 mm, dotted line: h=11 mm) and the static condensation method (solid line).

The crack opening and the stress σ_y is shown in Fig. 2.6 for three different mesh refinements. Because the enrichment function is based on a partition of unity, spurious crack opening is not observed even in the coarse mesh. The crack opening profiles for h= 2 mm almost coincide with the reference crack opening profiles so that the difference is indiscernible.

The stresses on the dashed line in Fig. 2.4(a) are plotted in Fig. 2.6. It can be seen that the change of the stress profiles as the crack advances in the fracture process zone is approximately self-similar. As the mesh is refined, the stress profiles converge to the reference profiles. The stress profiles for h=2 mm agree well with the reference profiles.
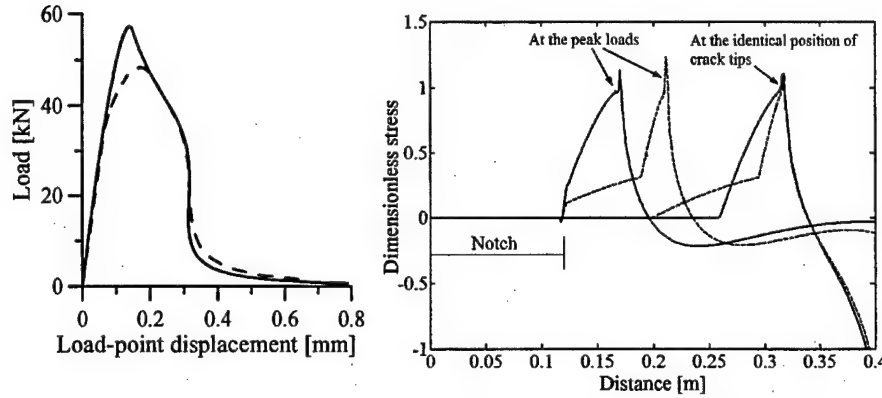
Fig. 2.7: Comparison of the results by the linear (solid line) and the bilinear (dashed line) softening law; the load-deflection histories (left) and the stresses σ_y (right).

Because of their simplicity, linear softening laws are frequently used. However, when post-peak behavior is important, nonlinear softening laws may be more accurate. The method developed can be applied to nonlinear softening laws as well as linear softening laws. One might think that if the fracture energy of two different softening law is identical, the load-deflection curve does not change.

In order to study the effect of cohesive laws, a bilinear softening law, shown in Fig. 2.4 (right), is taken into account. The tensile strength and the fracture energy of the bilinear softening law (dashed line) are the same as those of the linear softening law (solid line). The load-deflection histories for the two are compared in Fig. 2.7 (left). The peak load associated with the bilinear softening law is smaller than the linear one and the shapes of the load-deflection histories differ as well. As one can see in Fig. 2.7 (right), the fracture process zones are not fully developed at the peak loads, to which only the initial parts of the softening curves in Fig. 2.4 (right) contribute. Therefore the fracture energies associated with the peak loads are different although the fracture energies for the two softening laws are the same.

3. Adaptivity in the element free Galerkin (EFG) method

We have studied the adaptive procedures that provide accurate solutions to dynamic nonlinear with cohesive cracking problems with minimal user intervention. The key feature of the proposed methodologies are the generation of models with a prescribed level of accuracy via adaptivity.

The raison d'etre for meshfree methods is to totally avoid any mesh generation. Thus a true meshfree method should be able to start with a solid model or geometric model and provide a solution of the requisite accuracy. Obviously, adaptivity is a key ingredient in any such procedure, since in automatic model generation, user intervention in the assignment of refinement would be unacceptable.

The procedure proposed here combines meshfree methods with so-called Cartesian (or structured methods). In these methods, the arrangement of the nodes (or particles) is structured as shown in Fig. 3.2. Although at first such a combination appears illogical, since a key advantage of meshfree methods is their ability to handle arbitrary clouds of nodes, after careful consideration we concluded there is little reason to model objects with a random cloud of particles, and in fact, the construction of random clouds with effective fidelity would be more difficult than the construction of structured node sets. Furthermore, random node arrangements would complicate the implementation of adaptivity, post-processing and parallelization.

One could question the use of meshfree methods in a structured context; if the nodal arrangement is structured, it would appear that standard finite difference methods would be optimal. However, finite difference methods are quite unwieldy in treating the irregular arrangements of nodes that arise in an adaptive procedure. Furthermore, meshfree methods through partition of unity concepts enable the

8

method to incorporate features such as internal discontinuities, singular solutions, and handbook solutions. These features endow the methodology with powerful advantages: discontinuous partitions of unity can treat arbitrary cracks without remeshing, singular partitions of unity can treat elastic near tip fields for cracks and dislocations without mesh refinement, handbook solutions can treat holes and inclusions that are smaller than the scale of the discretization.

Some of these ideas have already been presented in the finite element context. Strouboulis et al. (2001) in the generalized finite element method introduced the concept of adding handbook solutions for subscale features. Belytschko et al. (2003) developed a structured finite element method based on implicit surface definitions with arbitrary internal features such as cracks and and sliding interfaces. Belytschko et al. (2003) showed how this methodology could be applied to topology optimization.

Another question the reader may pose is why use meshfree methods instead of higher order finite elements. Indeed spectral finite elements are extremely powerful for treating many problems. However, for the nonsmooth problems found in solid mechanics, such aselastic-plastic materials and contact-impact, p-adaptivity is inferior to h-adaptivity. Furthermore, the implementation of h-adaptivity for finite elements even in a structured mesh is much more difficult than for meshfree methods.

We will use the element-free Galerkin (EFG) meshfree method in this study. This method uses moving least square (MLS) approximations. We will not consider some recent methods such as radial basis functions and so called truly meshless methods. The former require multipolar methods for reasonable speed on large models. The truly meshless methods are more in the spirit of clouds of particles, which are not in the spirit of the methodology proposed here.

We have chosen a Total Lagrangian description. The momentum equation can then be written as

$$\int_{\Omega_0} \rho_0 \, \delta u_i \, \ddot{u}_i \, d\Omega_0 + \int_{\Omega_0} \frac{\partial u_i}{\partial x_i} \, P_{ij} \, d\Omega_0 - \int_{\Omega_0} \rho_0 \, \delta u_i \, b_i \, d\Omega_0 - \int_{\Omega_0} \delta u_i \, \bar{t}_i \, d\Gamma_0 = 0 \qquad (3.1)$$

where ρ_0 is the initial density, u_i are the displacements, P_{ij} are the nominal stresses, b_i are the body forces and $\bar{t}_i$ are the external forces. The test functions are approximated by

$$\delta u_i = \sum_{J \in S} \delta u_{iJ} \, \Phi_J(X_i) \qquad (3.2)$$

where the shape functions $\Phi_J(X_i)$ are the EFG shape functions. The integrals are evaluated by an integration based on a background mesh.

The adaptivity approach is based on an interpolation error. Regions with a large local error, i.e. high strain gradients, are refined. The refinement strategy is illustrated in Fig. 3.2. The cell is divided into four smaller cells of equal size. In our numerical studies large errors occurred if the size of the neighboring cells differs too much. Therefore, a cell is refined, if it shares more than two edges with a neighbor cell as shown in Fig. 3.2 where the last refinement step from Fig. 3.1 is chosen as source.

In dynamic problems, a lumped or diagonal mass matrix is used instead of a consistent one since it simplifies the computation. In particle methods, there exist different techniques to compute the masses of the particles. A common procedure is to assign the masses and volumes to the particles according to a Voronoi diagram (see Fig. 3.3) before beginning the time integration. Another way is to establish a diagonal mass matrix from the consistent mass matrix using the row sum technique.

If adaptivity takes place, it becomes necessary to recompute the new masses and volumes after every refinement step. It is computationally easier to compute the diagonal mass matrix from the consistent one, especially if particles are added in an irregular pattern. Therefore, we have chosen this approach.

If an incremental stress strain law is applied, the stresses have to be assigned to the new particles. Also values of the velocity have to be transformed to the new particles. All values are obtained by an MLS fit, i.e. via the approximation. Especially, when the particles are arranged in an irregular pattern, this procedure is straightforward. The new interpolation radius h is chosen according to the maximum distance of the neighbor particles. In the particle sums, an average of $h_{IJ} = 0.5(h_I + h_J)$ is calculated to obtain a symmetric interaction.

The response of notched concrete under dynamic loading have been studied. Here, we consider the beam as shown in Fig. 3.4. We compare again the crack pattern obtained with a continuum model and the discrete crack model. EFG with cell integration was taken to solve this problem. Fig. 3.5 shows the crack obtained from the simulation with a continuum damage model and the discrete crack model. It can be seen that the adaptive method refines around the path of the crack, so that a very accurate path can be obtained. Fig. 3. 6 illustrated the refinement of the crack close to the notch.
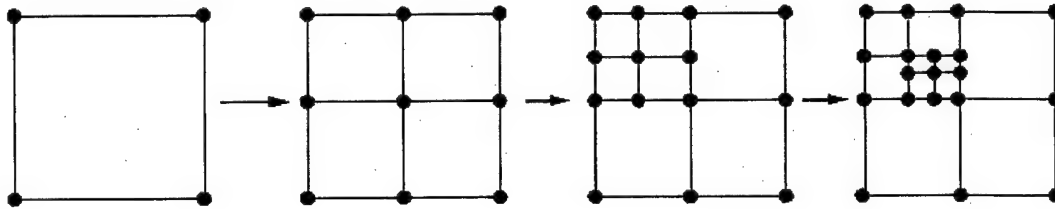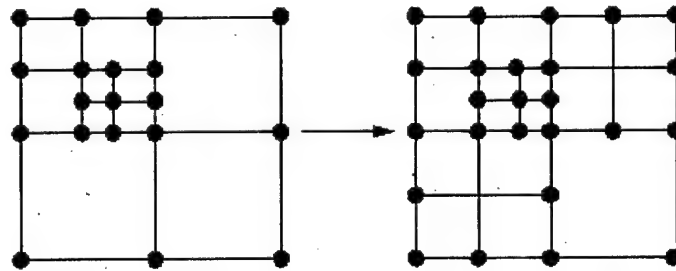

Fig. 3.1: Refinement strategy

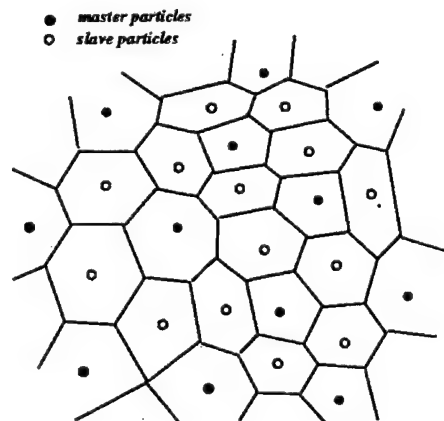**Fig. 3.2:** Refinement to create a smooth transition
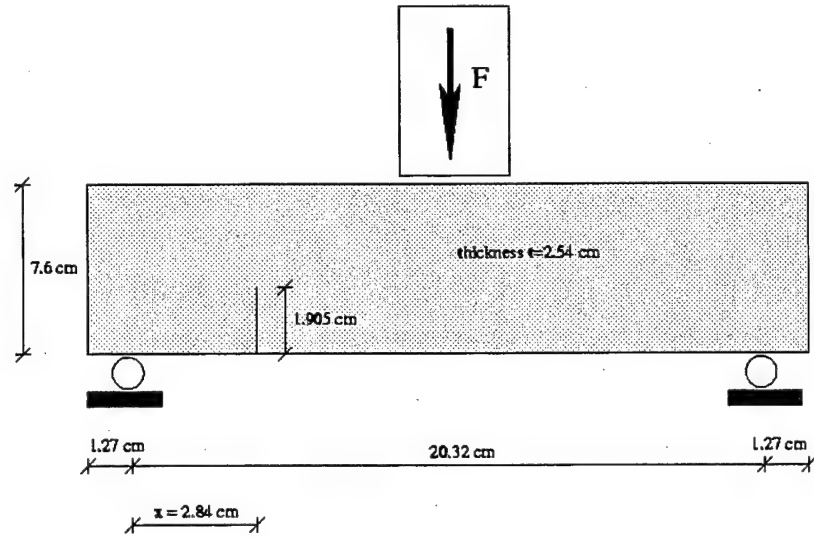

Fig. 3.3: Voronoi diagram

10

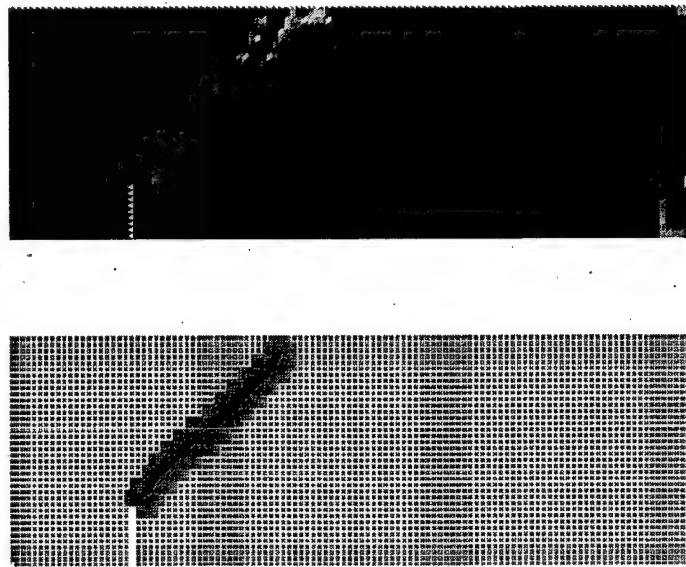**Fig. 3.4:** The notched concrete beam of John and Shah

Fig. 3.5: The crack pattern of the notched concrete beam in the numerical simulation
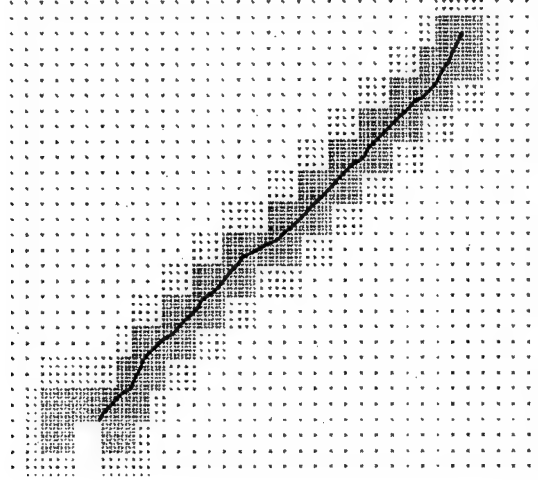
11

Fig. 3.6: Refinement around the crack

4. Domain decomposition

A method has been developed for coupling fine scale models of subdomains with coarse scale models. The essential feature of any such coupling is that it should not lead to spurious reflections off the interface. Direct linkages of fine and coarse scale models lead to nonphysical reflections because the impedance of the coarse scale model differs significantly from that of the fine scale model. In face, for frequencies above the cutoff frequency of the fine scale model, the coarse scale model appears almost as a rigid boundary condition.

The coupling method is based on overlapping domain decomposition techniques, see Belytschko and Xiao (2003). The essential idea is that on the overlapping domain, the fine scale solution is projected in each time step onto the coarse scale solution. This is accomplished by scaling the Hamiltonian within the bridging domain and constraining the velocities of the overlapping nodes by Lagrange multipliers.
The Hamiltonian is defined as:

$$H = K + E = \int_\Omega \frac{\mathbf{P}^2}{2\rho} + W(\mathbf{F})d\Omega \tag{4.1}$$

where $\mathbf{P}$ is the momentum, ρ is the density, $\mathbf{F}$ is the gradient of deformation, and W is the internal energy or strain energy.

The equations of motion can be written as:

$$\dot{\mathbf{x}} = \frac{\partial H}{\partial \mathbf{P}} \qquad \text{and} \qquad \dot{\mathbf{P}} = -\frac{\partial H}{\partial x} \tag{4.2}$$

The total Hamiltonian of Bridging domain multiscale method for FEM is written as the linear combination of Hamiltonian from fine mesh Ω^F and coarse mesh Ω^C of FEM, as shown in Fig. 4.2.

$$H = \beta H^F + (1 - \beta)H^C = \beta\left(K^F + E^F\right) + (1 - \beta)\left(K^C + E^C\right) \tag{4.3}$$

where β is a scalar parameter which ranges from 0 to 1 in bridging domain Ω^{int}. The bridging domain is also called overlapping domain.
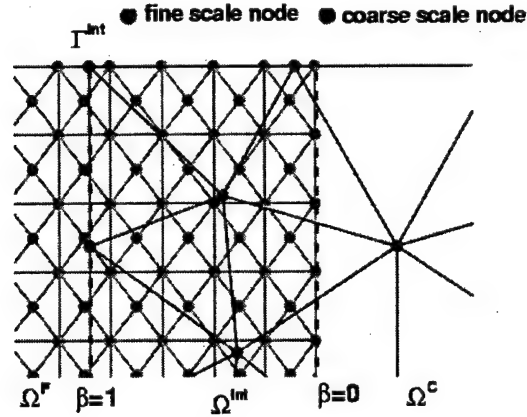
12

Fig. 4.1 : Overlapping domain of bridging domain multiscale method

The two models are constrained on the overlapping subdomain Ω^{int} by

$$\mathbf{g}_I = \{g_{il}\} = \{u_i(\mathbf{X}_I) - d_{il}\} = \left\{\sum_J N_J(\mathbf{X}_I)u_{iJ} - d_{il}\right\} = 0 \qquad (4.4)$$

i.e. the fine mesh displacements $\mathbf{d}$ conform to the coarse mesh displacements $\mathbf{u}$ at the discrete positions of the fine mesh nodes. The constraints are applied on the each component of the displacements.

When Lagrangian multiplier method is applied, the total Hamiltonian will be given as:

$$H_L = H + \lambda^T \mathbf{g} = H + \sum_I \lambda_I^T \mathbf{g}_I \qquad (4.5)$$

where λ is the vector of Lagrange multipliers which are assigned on the discrete fine mesh nodes in the bridging domain.

Then, the equations of motion are:

$$\dot{\mathbf{P}} = -\frac{\partial H_L}{\partial \mathbf{x}} \qquad (4.6)$$

i.e.

$$\overline{m}_I \ddot{\mathbf{d}}_I = \mathbf{f}_I^{ext} - \mathbf{f}_I^{int} - \sum_J \lambda_J^T \frac{\partial \mathbf{g}_J}{\partial \mathbf{d}_I} = \mathbf{f}_I^{ext} - \mathbf{f}_I^{int} - \mathbf{f}_I^L \qquad \text{in } \Omega^F$$

$$\overline{M}_I \ddot{\mathbf{u}}_I = \mathbf{F}_I^{ext} - \mathbf{F}_I^{int} - \sum_J \lambda_J^T \frac{\partial \mathbf{g}_J}{\partial \mathbf{u}_I} = \mathbf{F}_I^{ext} - \mathbf{F}_I^{int} - \mathbf{F}_I^L \qquad \text{in } \Omega^C$$

where

$$\overline{m}_I = \sum_J \int_{\Omega_0^F} \beta(\mathbf{X})N_I(\mathbf{X})N_J(\mathbf{X})d\Omega_0^F$$

$$\overline{M}_I = \sum_J \int_{\Omega_0^C} (1 - \beta(\mathbf{X}))N_I(\mathbf{X})N_J(\mathbf{X})d\Omega_0^C$$

$$\mathbf{f}_I^{int} = \int_{\Omega_0^F} \beta(\mathbf{X})\frac{\partial N_I(\mathbf{X})}{\partial \mathbf{X}}\mathbf{P}d\Omega_0^F$$

$$\mathbf{F}_I^{int} = \int_{\Omega_0^C} (1 - \beta(\mathbf{X}))\frac{\partial N_I(\mathbf{X})}{\partial \mathbf{X}}\mathbf{P}d\Omega_0^C$$

$$\mathbf{f}_I^{ext} = \int_{\Omega_0^F} \beta(\mathbf{X})N_I \rho_0 \mathbf{b} d\Omega_0^F + \int_{\Gamma_0^t} \beta(\mathbf{X})N_I \bar{\mathbf{t}} d\Gamma_0^t$$

$$\mathbf{F}_I^{ext} = \int_{\Omega_0^C} (1-\beta(\mathbf{X}))N_I \rho_0 \mathbf{b} d\Omega_0^C + \int_{\Gamma_0^t} (1-\beta(\mathbf{X}))N_I \bar{\mathbf{t}} d\Gamma_0^t$$

We developed an explicit algorithm based on central difference method to solve these equations of motion. Suppose we already know the accelerations, velocities and displacement for time step n. We first obtain the displacements at the next time step $n+1$.

$$\mathbf{u}_{I(n+1)} = \mathbf{u}_{I(n)} + \dot{\mathbf{u}}_{I(n)}\Delta t + \frac{1}{2}\ddot{\mathbf{u}}_{I(n)}\Delta t^2 \qquad in \quad \Omega_0^C$$

$$\mathbf{d}_{I(n+1)} = \mathbf{d}_{I(n)} + \dot{\mathbf{d}}_{I(n)}\Delta t + \frac{1}{2}\ddot{\mathbf{d}}_{I(n)}\Delta t^2 \qquad in \quad \Omega_0^M \tag{4.7}$$

The accelerations for next time step can be given from (4.6) without considering the force due to the constraints:

$$\ddot{\mathbf{d}}_{I(n+1)} = \frac{1}{\overline{m}_I}\left[\mathbf{f}_{I(n+1)}^{ext} - \mathbf{f}_{I(n+1)}^{int}\right] \qquad in \quad \Omega_0^F$$

$$\ddot{\mathbf{u}}_{I(n+1)} = \frac{1}{\overline{M}_I}\left[\mathbf{F}_{I(n+1)}^{ext} - \mathbf{F}_{I(n+1)}^{int}\right] \qquad in \quad \Omega_0^C \tag{4.8}$$

Then, we obtain the trial velocities:

$$\dot{\mathbf{d}}_{I(n+1)}^* = \dot{\mathbf{d}}_{I(n)} + \frac{1}{2}\left[\ddot{\mathbf{d}}_{I(n)} + \ddot{\mathbf{d}}_{I(n+1)}\right]\Delta t \qquad in \quad \Omega_0^M$$

$$\dot{\mathbf{u}}_{I(n+1)}^* = \dot{\mathbf{u}}_{I(n)} + \frac{1}{2}\left[\ddot{\mathbf{u}}_{I(n)} + \ddot{\mathbf{u}}_{I(n+1)}\right]\Delta t \qquad in \quad \Omega_0^C \tag{4.9}$$

Alternatively, the velocities at time step $n+1$ can be expressed as:

$$\dot{\mathbf{d}}_{I(n+1)} = \dot{\mathbf{d}}_{I(n)} + \frac{1}{2}\left[\ddot{\mathbf{d}}_{I(n)} - \overline{m}_I^{-1}\mathbf{f}_{I(n)}^L + \ddot{\mathbf{d}}_{I(n+1)} - \overline{m}_I^{-1}\mathbf{f}_{I(n+1)}^L\right]\Delta t$$

$$= \dot{\mathbf{d}}_{I(n+1)}^* - \overline{m}_I^{-1}\Delta t \sum_J \mathbf{G}_{JI}^F \lambda_J \tag{4.10}$$

$$\dot{\mathbf{u}}_{I(n+1)} = \dot{\mathbf{u}}_{I(n)} + \frac{1}{2}\left[\ddot{\mathbf{u}}_{I(n)} - \overline{M}_I^{-1}\mathbf{F}_{I(n)}^L + \ddot{\mathbf{u}}_{I(n+1)} - \overline{M}_I^{-1}\mathbf{F}_{I(n+1)}^L\right]\Delta t$$

$$= \dot{\mathbf{u}}_{I(n+1)}^* - \overline{M}_I^{-1}\Delta t \sum_J \mathbf{G}_{JI}^C \lambda_J \tag{4.11}$$

where $\mathbf{G}_{LJ}^C = \left[\frac{\partial \mathbf{g}_L}{\partial \mathbf{u}_J}\right] = [N_{JL}\mathbf{I}]$, $\mathbf{G}_{LI}^F = \left[\frac{\partial \mathbf{g}_L}{\partial \mathbf{d}_I}\right] = [-\delta_{IL}\mathbf{I}]$. $\lambda_I = \frac{1}{2}\left[\lambda_{I(n)} + \lambda_{I(n+1)}\right]$ denote the unknown Lagrange multipliers. The above velocities satisfy the constraints (4) in time derivative form

$$\dot{\mathbf{g}}_{I(n+1)} = \dot{\mathbf{u}}(\mathbf{X}_I)_{(n+1)} - \dot{\mathbf{d}}_{I(n+1)} = \sum_J N_I(\mathbf{X}_J)\dot{\mathbf{u}}_{J(n+1)} - \dot{\mathbf{d}}_{I(n+1)} \tag{4.12}$$

Substituting (4.10) and (4.11) into (4.12), the unknown Lagrange multipliers can be obtained by solving the following equations:

$$\sum_L \mathbf{A}_{IL}\lambda_L = \mathbf{g}_I^* \tag{4.13}$$

14

where

$$\mathbf{A}_{IL} = \Delta t \overline{M}_I^{-1} \sum_J N_{JI} \mathbf{G}_{LJ}^C - \Delta t \overline{m}_I^{-1} \mathbf{G}_{LI}^F \; , \; \mathbf{g}_I^* = \sum_J N_{JI} \dot{\mathbf{u}}_J^* - \dot{\mathbf{d}}_I^*$$

After obtaining the Lagrange multipliers, the corrected velocities at time $n+1$ are given in (4.10) and (4.11).

To study the effectiveness of this method, a wave propagation problem in a one-dimensional rod is studied for both the bridging domain coupling method and an edge-to-edge coupling method. The initial wave is a combination of high frequency wave and low frequency wave. Spurious wave reflection occurs when edge-to-edge coupling method is used as shown in Fig. 4.2(b). However, Fig. 4.2(a) shows that bridging domain coupling method can eliminate the wave reflection without any additional filtering or viscosities. Fig. 4.3 shows the histories of energy in fine mesh domain or coarse mesh domain. After the low frequency wave passes through the coarse mesh domain, similar energies pass through whatever coupling method is used. In fine mesh domain, the energy of high frequency remains from edge-to-edge coupling method due to the spurious wave reflection, but it is reduced to zero from bridging domain coupling method as shown in Fig. 4.3(a).
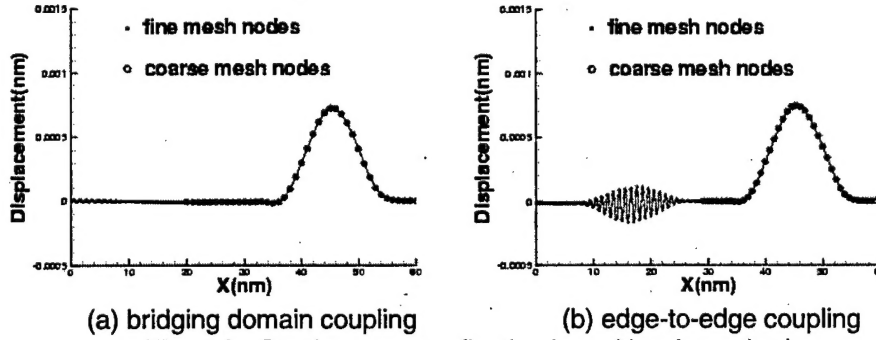

(a) bridging domain coupling   (b) edge-to-edge coupling

Fig. 4.2 : Spurious wave reflection in multiscale methods

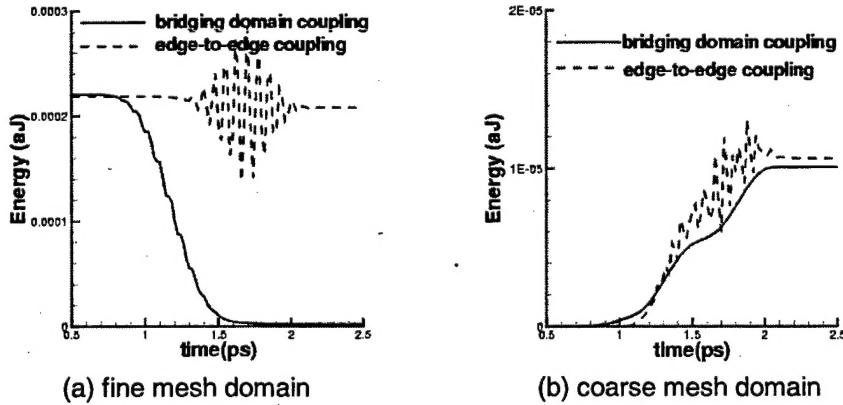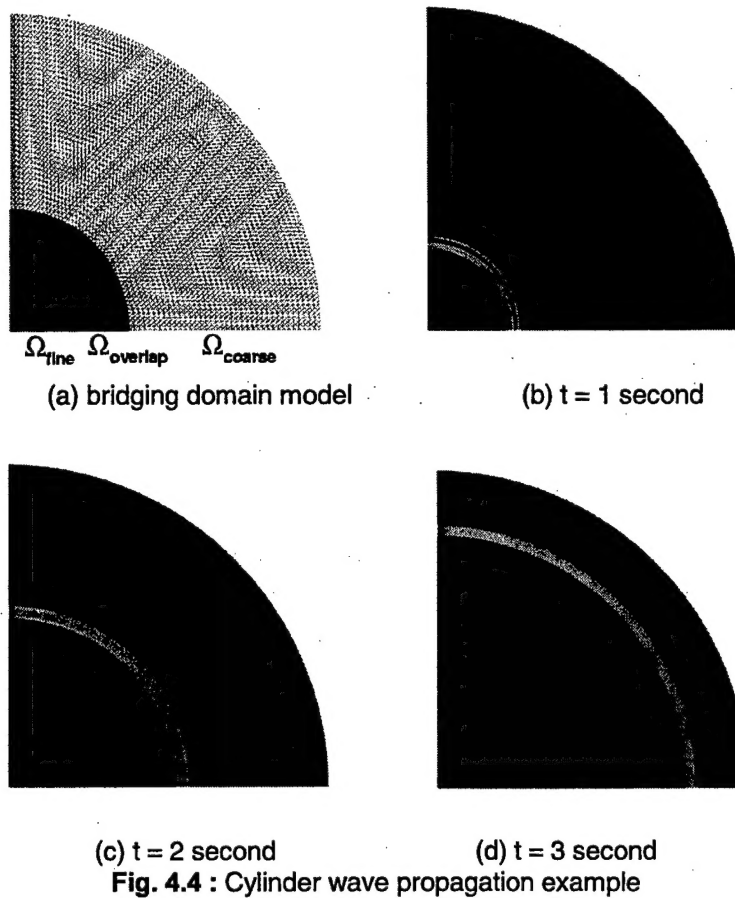(a) fine mesh domain   (b) coarse mesh domain

Fig. 4.3 : Histories of energy

Cylindrical wave propagation in two-dimensional plate is shown in Fig. 4.4. Fig. 4.4(a) shows the bridging domain coupling model which we use here. Fig. 4.4 (b)-(d) show the configurations of wave propagation at three different times. There is almost no spurious wave reflection when cylinder wave propagates from fine mesh domain to coarse mesh domain.

15

(a) bridging domain model   (b) t = 1 second

(c) t = 2 second   (d) t = 3 second

Fig. 4.4 : Cylinder wave propagation example

5. References

Belytschko, T. and Black, T. (1999). Elastic crack growth in finite elements with minimal remeshing. *International Journal for Numerical Methods in Engineering*, 45(5): 601-620.

Belytschko, T. and Mish, K. (2001). Computability in non-linear solid mechanics. *International Journal for Numerical Methods in Engineering*. 52:3-21.

Belytschko, T., Moes, N., Usui, S., and Parimi, C. (2001). Arbitrary discontinuities in finite elements. *International Journal for Numerical Methods in Engineering*, 50(4): 993-1014.

Belytschko, T., Parimi, C., Moes, N. (2003). Structured extended finite element methods for solids defined by implicit surfaces, *International Journal for Numerical Methods in Engineering*, 56(4), 609-635.

Belytschko, T., and Xiao, S. P. (2003). Coupling methods for continuum model with molecular model, *International Journal for Multiscale Computational Engineering,* 1(1), 115-126.

Belytschko, T., and Xiao, S. (2002). Stability Analysis of Particle Methods with Corrected Derivatives. *Computers and Mathematics with Applications*, 43: 329-350.

Chen, H. (2003). *Enriched finite element methods and its applications*. Ph. D. thesis, Northwestern University.

Chessa, J., Wang, H., and Belytschko, T. (2003). On the construction of blending elements for local partition of unity enriched finite elements. *International Journal for Numerical Methods in Engineering*, 57(7): 1015—1038.

Li, S., Qian, D., Liu, W.K., and Belytschko, T. (2001). A meshfree contact-detection algorithm. *Computer Methods in Applied Mechanics and Engineering*, 190: 3271-3292.

Li, S., Liu, W.K., Rosakis, A.J., Belytschko, T., and Hao, W. (2002). Mesh-free Galerkin simulations of dynamic shear band propagation and failure mode transition. *International Journal of Solids and Structures*, 39: 1213-1240.

Moes, N., and Belytschko, T. (2002). Extended finite element method for cohesive crack growth. *Engineering Fracture Mechanics*, 69 (7): 813-834.

Oden, J.T., Belytschko, T., Babuska, I., and Hughes, T.J.R. (2003). Research directions in computational mechanics. *Computer Methods in Applied Mechanics and Engineering*, 192: 913-922.

Stazi, F., Budyn, E., Chessa, J., and Belytschko, T. (2003). XFEM for fracture mechanics with quadratic elements. *Computational Mechanics*, 31: 38-48.

Strouboulis T., Copps K., Babuska I. (2001). The generalized finite element method, Comput. Methods *Applied Mechanics in Engineering*, 190(32-33), 4081-4194.

Ventura, G., Xu, J.X., and Belytschko, T. (2002). A vector level set method and new discontinuity approximations for crack growth by EFG. *International Journal for Numerical Methods in Engineering*, 54 (6): 923-944.

Wells, G. N., and Sluys, L. J. (2001). A new method for modelling cohesive cracks using finite elements. *International Journal for Numerical Methods in Engineering*, 50(12): 2667-2683.

Zi, G., and Bazant, Z. P. (2003). Eigenvalue method for computing size effect of cohesive cracks with residual stress, with application to kink bands in composites. *International Journal of Engineering Science*, 41(13-14): 1519-1534.